ACS MATERIALS Au
AN OPEN ACCESS JOURNAL OF THE AMERICAN CHEMICAL SOCIETY

pubs.acs.org/materialsau

Article

Solar-Driven Generation of Hydrogen Peroxide on Phenol–Resorcinol–Formaldehyde Resin Photocatalysts

Yasuhiro Shiraishi,* Kanako Miura, Masahiro Jio, Shunsuke Tanaka, Satoshi Ichikawa, and Takayuki Hirai

Cite This: *ACS Mater. Au* 2022, 2, 709–718

Read Online

ACCESS | Metrics & More | Article Recommendations | Supporting Information

ABSTRACT: Photocatalytic generation of H_2O_2 from water and O_2 under sunlight is a promising artificial photosynthesis reaction to generate renewable fuel. We previously found that resorcinol–formaldehyde resin powders prepared with a high-temperature hydrothermal method become semiconductors comprising π-conjugated/π-stacked benzenoid–quinoid donor–acceptor resorcinol units and are active for photocatalytic H_2O_2 generation. Here, we have prepared phenol–resorcinol–formaldehyde resins with small amounts of phenol (~5 mol % relative to resorcinol), which show enhanced photocatalytic activity. Incorporating phenol bearing a single –OH group in the resin matrices relaxes the restriction on the arrangement of the aromatic rings originating from the H-bonding interactions between the resorcinol –OH groups. This creates stronger donor–acceptor π-stacking and increases the electron conductivity of the resins. We have demonstrated that simulated sunlight illumination of the resins in water under an atmospheric pressure of O_2 stably generated H_2O_2 with more than 0.9% solar-to-chemical conversion efficiency.

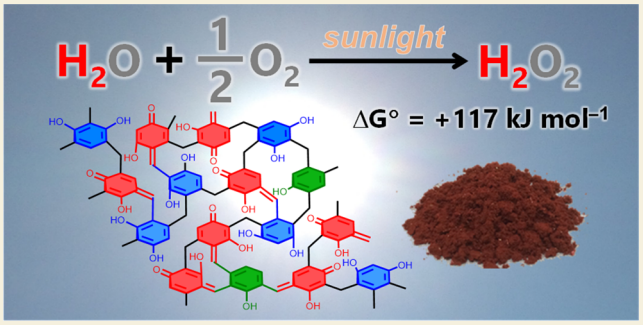

KEYWORDS: *photocatalysis, hydrogen peroxide, solar, Water, organic semiconductor*

INTRODUCTION

Artificial photosynthesis, the conversion of abundant resources into fuels by sunlight, is an important technology for generating renewable energy required to build a sustainable society. Several photoreactions involving water splitting (H_2 production),[1,2] CO_2 reduction (CO, HCOOH, CH_3OH, or CH_4 production),[3,4] and N_2 reduction (NH_3 production)[5,6] are under research for the generation of solar fuels. Recently, hydrogen peroxide (H_2O_2) has gained interest as a storable and transportable liquid fuel that generates electricity in fuel cells.[7] Most importantly, H_2O_2 can be generated from water and O_2 by photocatalysis.[8−10] Promoting the oxidation of water by the valence band holes (VB h^+) (eq 1) and reduction of O_2 by the conduction band electrons (CB e^-) (eq 2) generate H_2O_2 (eq 3) under ambient conditions. Therefore, sunlight-driven H_2O_2 generation is a promising strategy to produce a solar fuel by artificial photosynthesis.

$$H_2O \rightleftharpoons 1/2O_2 + 2H^+ + 2e^- \ (+1.23\ \text{V vs NHE, pH 0}) \quad (1)$$

$$O_2 + 2H^+ + 2e^- \rightleftharpoons H_2O_2 \ (+0.68\ \text{V vs NHE, pH 0}) \quad (2)$$

$$H_2O + 1/2O_2 \xrightarrow{h\nu} H_2O_2 \ (\Delta_r G^\circ = +116.7\ \text{kJ mol}^{-1}) \quad (3)$$

Several photocatalytic systems have been proposed for this reaction,[8−10] but their performances are insufficient. They exhibit a low activity for the water oxidation (eq 1), a low selectivity for the two-electron O_2 reduction (eq 2), and a subsequent decomposition of the generated H_2O_2 by absorbing ultraviolet light or by photocatalytic oxidation (the reverse reaction of eq 2). Thus, designing catalysts that efficiently promote water oxidation and O_2 reduction under visible light while being less active toward H_2O_2 decomposition remains a challenge.

We previously found that resorcinol–formaldehyde (RF) resins,[11] which had been considered as insulating polymers,[12−14] act as n-type semiconductors when prepared by a high-temperature hydrothermal method and are active for photocatalytic H_2O_2 generation.[15] This synthesis produces resins consisting of quinoid forms of resorcinol, which are π-conjugated with benzenoid forms of resorcinol via methine linkers (Scheme 1a).[16,17] The benzenoid–quinoid π-conjugated donor–acceptor (D–A) units have a small highest

Received: June 6, 2022
Revised: July 22, 2022
Accepted: August 9, 2022
Published: August 18, 2022

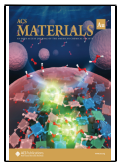

https://doi.org/10.1021/acsmaterialsau.2c00041
ACS Mater. Au 2022, 2, 709–718

Scheme 1. (a) Crosslinking, (b) π-Conjugated/π-Stacked D−A Structure, and (c) Electronic Band Structure of RF Resins; (d) Crosslinking, (e) π-Conjugated/π-Stacked D−A Structure, and (f) Electronic Band Structure of PRF Resins

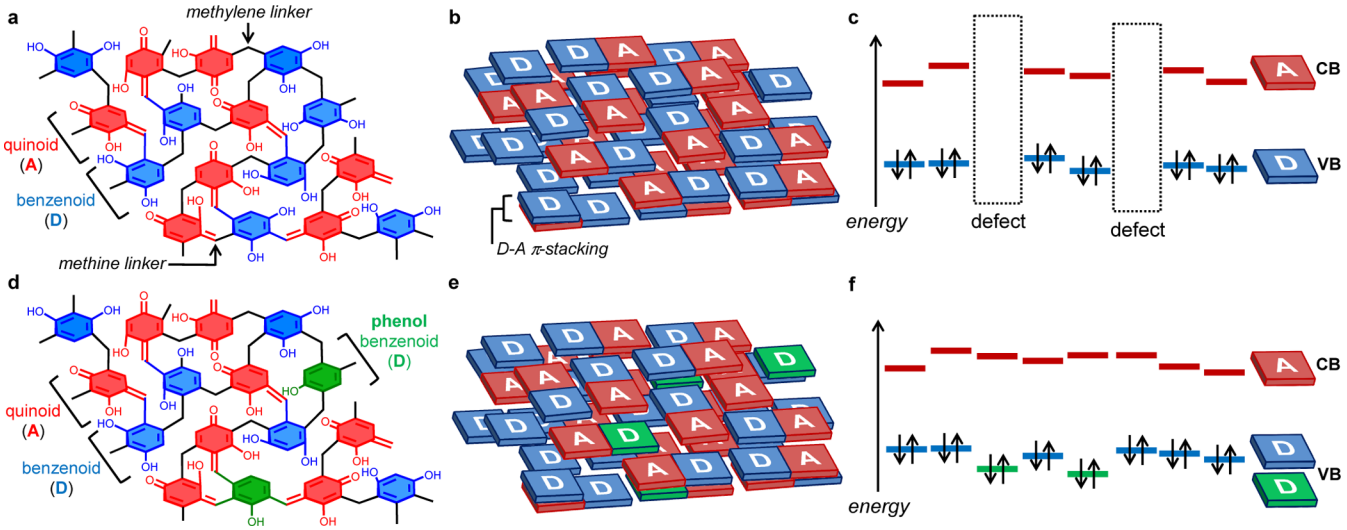

occupied molecular orbital−lowest unoccupied molecular orbital (HOMO−LUMO) gap. Their π-stacking interactions (Scheme 1b) hybridize the HOMO−LUMO levels, thereby creating semiconducting bands (Scheme 1c) with low band gap energies (E_{bg} = ∼1.5 eV), where the D and A units form the VB and CB, respectively. The low-E_{bg} resins efficiently promote water oxidation and O_2 reduction while being less active toward decomposing the generated H_2O_2. Photoexcitation of the resins suspended in water under an atmospheric pressure of O_2 produced H_2O_2 with a solar-to-chemical conversion (SCC) efficiency being ∼0.7%,[16] which is the highest efficiency among the reported powder catalysts for the artificial photosynthesis reactions.[1−8] Thus, low-E_{bg} metal-free resins that can be readily prepared using inexpensive reagents may open new pathways for H_2O_2 generation.

The next challenge is to improve the photocatalytic activity of RF resins. The resins are amorphous; therefore, improving the e^- conductivity is a critical approach for activity enhancement. In our previous work, we prepared RF resin powders doped with poly(3-hexylthiophene-2,5-diyl) (P3HT), a conducting polymer.[17] The RF/P3HT resin facilitates efficient transfer of the photogenerated CB e^- through the doped P3HT. This enhances h^+−e^- charge separation and promotes efficient water oxidation and O_2 reduction. The SCC efficiency for the H_2O_2 generation on the RF/P3HT resin increased to ∼1.0%. Increasing the e^- conductivity of the RF resin is therefore a powerful approach toward photocatalytic H_2O_2 generation. However, P3HT is expensive and is difficult for practical applications. It is therefore necessary to develop a new method to increase e^- conductivity using inexpensive reagents.

It has been reported that H-bonding interactions within polymer materials strongly affect the configuration and π-stacking interactions of the aromatic units.[18,19] The RF resins consist of resorcinols bearing two −OH groups, which are strongly associated in the resins via H-bonding interactions, as confirmed by density functional theory (DFT) calculations.[15] These −OH interactions may restrict the arrangement of the benzenoid and quinoid units within the resin matrices and partly weaken the D−A π-stacking. This probably creates dissipated semiconducting bands (Scheme 1c), leading to a low e^- conductivity of the resins. Thus, connecting the dissipated bands is important for ensuring efficient charge transport. In this context, decreasing the number of −OH groups within the RF resin matrices is a key strategy for weakening the H-bonding interactions and strengthening the D−A π-stacking.

RF resins are the primary adhesives used in the manufacture of laminated wood because of their water-resistant properties.[20] Phenol is cheaper than resorcinol and is usually mixed during the RF adhesive synthesis.[21] The phenol−resorcinol−formaldehyde (PRF) resins exhibit excellent cold-set bonding performance;[22] currently, the resins prepared with 80−90 mol % phenol and 10−20 mol % resorcinol are the most widely used adhesives.[23] It is noted that phenol possesses a single −OH group. Thus, we hypothesized that phenol, if doped within the RF resins, may affect the π-stacking of the D−A units and the e^- conductivity.

Herein, we report the enhanced activity for photocatalytic H_2O_2 generation on the PRF resins prepared under high-temperature hydrothermal conditions. In particular, the resins prepared using a mixture of ∼5 mol % phenol and ∼95 mol % resorcinol exhibited an activity that was 1.5 times higher than that of the RF resin. Polycondensation of resorcinol with small amounts of phenol bearing a single −OH group produces resins that homogeneously contain benzenoid-type phenol units (Scheme 1d,e). This weakens the H-bonding between the −OH groups within the resins and relaxes the restriction on the arrangement of the aromatic rings. This, in turn, leads to stronger π-stacking of the D−A units and reduces the number of defects, creating continuous semiconducting bands (Scheme 1f). Therefore, the e^- conductivity of the resins increases, which is conducive to efficient water oxidation and O_2 reduction. In addition, simulated sunlight illumination of the resins in water with O_2 stably generated H_2O_2 with more than 0.9% SCC efficiency, which is comparable to the efficiency on the RF/P3HT resin.[17]

RESULTS AND DISCUSSION

Preparation of the Resins

The P_xR_yF resin powders were prepared under acid-catalyzed high-temperature hydrothermal conditions identical to those of

https://doi.org/10.1021/acsmaterialsau.2c00041
ACS Mater. Au 2022, 2, 709−718

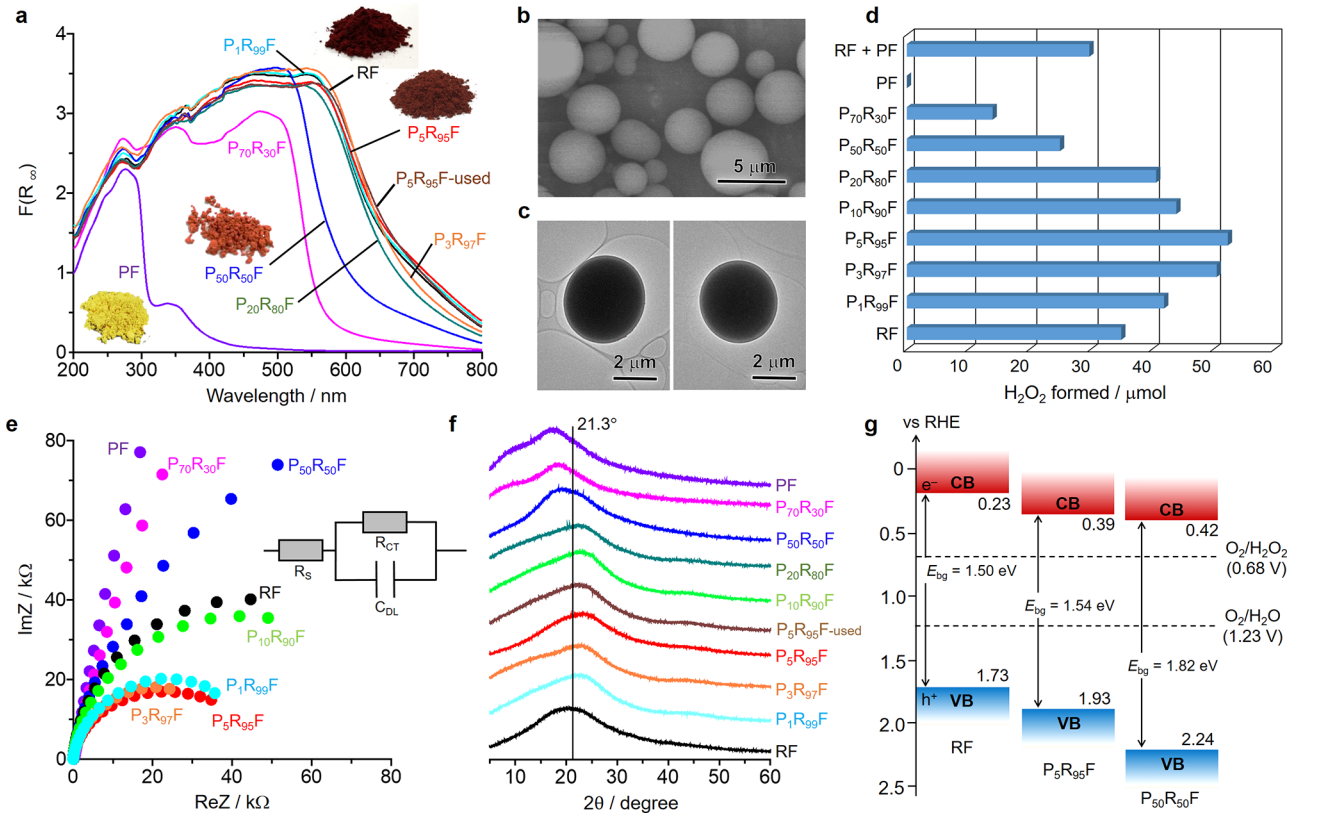

Figure 1. (a) Diffuse reflectance ultraviolet−visible spectra of the resins. (b) SEM and (c) TEM micrographs of the $P_5R_{95}F$ resin. (d) Amount of H_2O_2 generated during 6 h of photoirradiation on the respective resins. Conditions: water (30 mL), resin (50 mg), O_2 (1 bar), $\lambda > 420$ nm (Xe lamp), temperature (298 K). (e) Electrochemical impedance spectroscopy Nyquist plots of the resins measured in 0.1 M Na_2SO_4 under photoirradiation at a bias of 1.0 V (vs Ag/AgCl), where the circuit model involves ohmic resistance (R_S), double-layer capacitance (C_{DL}), and charge transfer resistance (R_{CT}). (f) Powder X-ray diffraction and (g) electronic band structures of the resins.

the RF resin,[16] where x and y are the mole ratios of phenol and resorcinol used for resin preparation, respectively ($x + y = 100$). Briefly, a phenol/resorcinol mixture, formaldehyde, and oxalic acid were added to pure water in a 20:40:1 mole ratio. The solutions were treated under hydrothermal conditions at 523 K for 12 h. Washing of the formed solids with acetone, followed by drying in vacuo yielded P_xR_yF resin powders (see details: Supporting Information).

The P_xR_yF resins obtained with small amounts of phenol ($x \leq 20$) are red-black powders (Figure 1a), similar to those of RF.[16] Increasing the phenol amounts leads to fading of the color, where the PF resin prepared without resorcinol is a light-yellow powder. Scanning electron microscopy (SEM) observations revealed that the P_xR_yF resins were spherical particles (Figures S1, Supporting Information), as was the case for RF.[16] Further, the $P_5R_{95}F$ resin consisted of 2−5 μm spheres (Figure 1b). Transmission electron microscopy (TEM) observations of $P_5R_{95}F$ (Figure 1c) and its images obtained at different angles (Figure S2) confirmed the formation of spherical particles. Dynamic light scattering (DLS) measurement (Figure S3) showed that the average hydrodynamic diameter of the $P_5R_{95}F$ particles (2.9 μm) was similar to that of RF (2.9 μm). In contrast, increasing the phenol amounts (x) produced larger resin particles, where the average diameters of $P_{50}R_{50}F$ and PF particles were 4.7 and 7.1 μm, respectively. The acid-catalyzed polycondensation is triggered by the nucleophilic addition of protonated formaldehyde to an aromatic ring.[14] The nucleophilicity of phenol is lower than that of resorcinol because one less −OH group lowers the electron density of the aromatic ring. The less reactive phenol undergoes polycondensation at a slower rate,[24] thereby producing larger resin particles. Further, the N_2 adsorption/desorption analysis of $P_5R_{95}F$ exhibited a type III isotherm similar to that of RF (Figure S4), indicating the formation of nonporous particles; the specific surface area of $P_5R_{95}F$ (0.68 $m^2\ g^{-1}$) is similar to that of RF (1.02 $m^2\ g^{-1}$). The above results suggest that P_xR_yF resins prepared with higher amounts of phenol are larger-sized particles while those prepared with lower amounts (~5 mol % phenol) have sizes and surface areas similar to those of RF.

Activity and Conductivity of the Resins

The photoreactions were performed by irradiating the resin (50 mg) suspended in water (30 mL) with visible light ($\lambda >$ 420 nm) using an Xe lamp (Figure S5), under 1 bar of O_2 at 298 K with magnetic stirring. Figure 1d shows the amount of H_2O_2 generated on the catalysts during 6 h of photoirradiation. RF produced 35 μmol H_2O_2, whereas PF showed almost no activity. We observed that the activity of the resins depended on the amount of phenol used for resin preparation. The resins prepared with small amounts of phenol ($x \leq 10$) exhibited a higher activity than that of RF, with $P_5R_{95}F$ showing the highest activity (53 μmol; ~1.5 times higher than that of RF). However, further addition of phenol decreased the activity. Additionally, the physical mixture of RF and PF (95/5 wt/wt) did not show any activity enhancement. These data indicate that ~5 mol % phenol is optimal for generating high amounts of H_2O_2.

https://doi.org/10.1021/acsmaterialsau.2c00041
ACS Mater. Au 2022, 2, 709−718

The superior activity of the $P_5R_{95}F$ resin is ascribed to its increased e^- conductivity, which enhances the separation of the h^+-e^- charges, thereby catalyzing efficient water oxidation and O_2 reduction. This was confirmed by electrochemical impedance spectroscopy (EIS) measurements using resin-loaded fluorine tin oxide (FTO) electrodes under photo-irradiation. The EIS Nyquist plots (Figure 1e) indicate that the resins prepared with small amounts of phenol ($x \leq 10$) show a charge transfer (CT) resistance (R_{CT}) lower than that of RF. $P_5R_{95}F$ showed the lowest R_{CT}, and the resins prepared with larger amounts of phenol ($x \geq 10$) showed increased R_{CT}. This trend agrees with that of the photocatalytic activity (Figure 1d), confirming that enhanced e^- conductivity critically affects the activity. The photocurrent response of the resin-loaded FTO (Figure S6) showed that the current density of $P_5R_{95}F$ was larger than that of RF, further confirming the enhanced h^+-e^- charge separation.

Compositions and Structures of the Resins

The diffuse reflectance ultraviolet−visible (DR UV−vis) spectra (Figure 1a) reveal that the resins prepared with small amounts of phenol ($x \leq 10$) exhibit broader absorption spectra that extend to ∼800 nm, similar to those of RF,[16] which is ascribed to the CT transitions of π-conjugated/π-stacked D−A units. In contrast, resins prepared with larger amounts of phenol ($x \geq 20$) showed blue-shifted absorption. In particular, the PF resin shows almost no absorption in the visible region,[25] indicating almost no D−A interaction within this resin. These data imply that the phenol incorporated within the resin does not form a quinoid (A) unit; therefore, PF may lack the D−A semiconducting property and may be inactive for photocatalysis (Figure 1d). The lack of a quinoid (A) unit in PF was confirmed by infrared (IR) spectroscopy (Figure S7), as the quinoid C═O band (1650 cm^{-1}) was absent, whereas it was observed in the spectra of RF, $P_5R_{95}F$, and $P_{50}R_{50}F$. Dipolar-decoupling magic-angle spinning ^{13}C nuclear magnetic resonance (DD/MAS/^{13}C NMR) spectra of the resins also confirmed this (Figures 2 and S8); the spectra consist of 14 components (**a**−**n**).[26−28] $P_5R_{95}F$ and $P_{50}R_{50}F$ showed quinoid C═O (**b**)[29] and the corresponding methine ═C− (**e**)[30] carbons with similar areas, confirming quinoid (A) formation. In contrast, PF did not show these peaks, indicating that the phenol incorporated within the resins exists in the benzenoid (D) form (Scheme 1d).

Table 1 presents the carbon compositions of the resins as determined by NMR. It must be noted that X-ray photoelectron spectroscopy (XPS) of the resins at the C 1s (Figure S9) and O 1s levels (Figure S10) showed C−O and C═O carbons.[31] The C−O/C═O ratios of the resins determined by the O 1s spectra agreed with those determined by NMR (Table S1), confirming the accuracy of the determined compositions (Table 1). RF, $P_5R_{95}F$, $P_{50}R_{50}F$, and PF exhibit similar compositions consisting of aromatics (∼68%), linkers (∼24%), and residual groups (∼8%). Further, the ratio of the number of linker carbons to the number of aromatic rings is ∼2; therefore, the average number of linkers on an aromatic ring is ∼3 because a linker connects two aromatic rings. This indicates that these resins have similar crosslinking degrees (Scheme 1a,d). In addition, the benzenoid/quinoid (D/A) ratio of $P_5R_{95}F$ (52/48) was similar to that of RF, suggesting that both the resins contain a nearly equal number of D/A units; this is in agreement with their similar absorption spectra (Figure 1a). In contrast, the D/A ratios of $P_{50}R_{50}F$ and PF were 74/26 and 100/0, respectively, which also agreed with the blue-shifted absorption spectra. The data indicate that the phenol incorporated into the resins exists in the benzenoid (D) form (Scheme 1d).

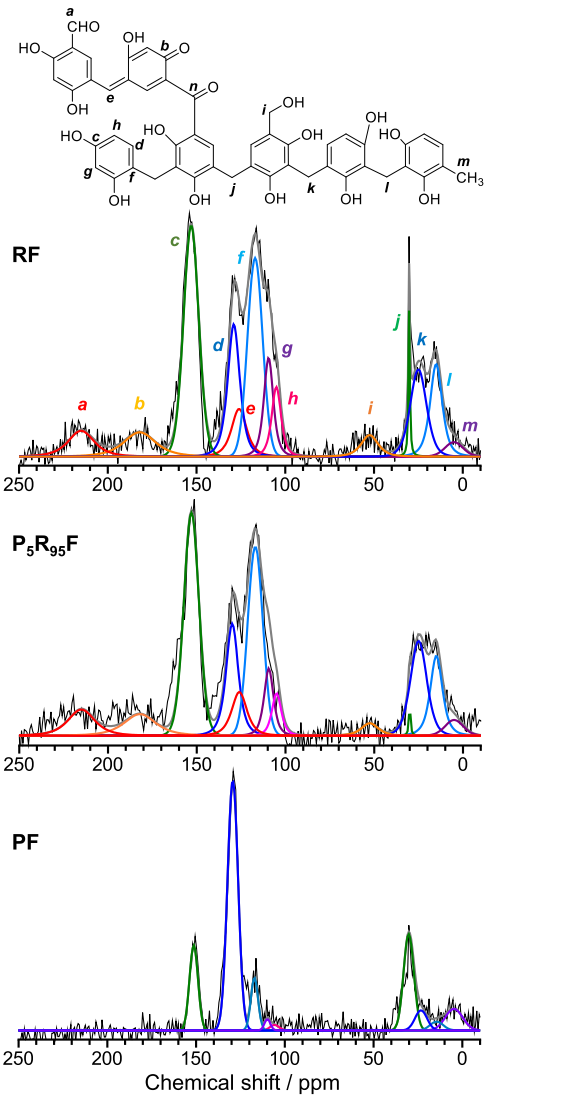

Figure 2. DD/MAS/^{13}C NMR spectra of the resins. (**a**) Aldehyde (215 ppm), (**b**) quinone C═O (182 ppm), (**c**) resorcinol C−OH (153 ppm), (**d**) non-substituted resorcinol at the meta position (130 ppm), (**e**) methine (126 ppm), (**f**) substituted resorcinol (117 ppm), non-substituted resorcinol at (**g**) para (110 ppm) and (**h**) ortho positions (105 ppm), (**i**) methylol (55 ppm), methylene substituted to (**j**) 4,4′- (30 ppm), (**k**) 2,4′- (20 ppm), and (**l**) 2,2′-positions of resorcinol (10 ppm), and (**m**) methyl (5 ppm).

During acid-catalyzed polycondensation (Scheme 2), the nucleophilic addition of protonated formaldehyde to resorcinol or phenol produces methylols. Their protonation and subsequent dehydration generate benzyl carbonium ions. The nucleophilic addition of the ions to an aromatic ring produces methylene linkages.[12−14] The high-temperature hydrothermal conditions lead to deprotonation of the ions to form quinone methide intermediates,[32] which add to an aromatic ring to yield methine-linked (π-conjugated) A units. The activation energy of quinone methide formation for phenol is 20−30 kJ mol^{-1} higher than that for resorcinol because of its lower nucleophilicity.[33] Thus, phenol rarely forms quinone methide, resulting in no formation of the quinoid (A) unit. Therefore,

https://doi.org/10.1021/acsmaterialsau.2c00041
ACS Mater. Au 2022, 2, 709−718

Table 1. Carbon Compositions of Resins[a]

resin	aromatics/% (**b**, **c**, **d**, **f**, **g**, **h**)	linkers/%			residual groups/%			benzenoid/quinoid[b]	linker/aromatic ring[c]
		methylene (**j**, **k**, **l**)	methine (**e**)	ketone (**n**)	aldehyde (**a**)	methylol (**i**)	methyl (**m**)		
RF	67.1	18.7	5.0	0	5.1	2.5	1.6	52.0/48.0	2.12
$P_5R_{95}F$	66.7	19.2	5.1	0	5.4	1.6	2.0	52.1/47.9	2.19
$P_5R_{95}F$[d]	67.0	15.9	5.2	3.1	5.8	0.4	2.5	52.4/47.6	2.16
$P_{50}R_{50}F$	68.4	20.4	3.1	0	4.2	0.5	3.3	74.2/25.8	1.89
PF	68.8	24.5	0	0	0	0	6.7	100/0	2.04

[a]Determined by NMR (Figures 2 and S8). The letters in the parentheses show the carbon types (Figure 2). [b]Mole fraction of the quinoid units was determined from the peak areas using the following equation

$$\%\ \text{quinoid} = \left(\frac{[\text{quinone C = O carbon } (\mathbf{b})] \times 6 \times 100}{[\text{all carbons } (\mathbf{a} - \mathbf{n})]} \Big/ [\text{all aromatic carbons } (\mathbf{b}, \mathbf{c}, \mathbf{d}, \mathbf{f}, \mathbf{g}, \mathbf{h})] \right) \times 100$$

[c]The ratio of the number of linker carbons to the number of aromatic rings was determined using the following equation

$$\text{linker/aromatic ring} = \frac{[\text{all linker carbons } (\mathbf{e}, \mathbf{j}, \mathbf{k}, \mathbf{l}, \mathbf{n})]}{[\text{all aromatic carbons } ((\mathbf{b}, \mathbf{c}, \mathbf{d}, \mathbf{f}, \mathbf{g}, \mathbf{h})]} \times 6$$

[d]$P_5R_{95}F$ resin recovered after photoreaction for 5 h in water with O_2 (Figure 5a).

Scheme 2. Proposed Mechanism for Acid-Catalyzed Polycondensation

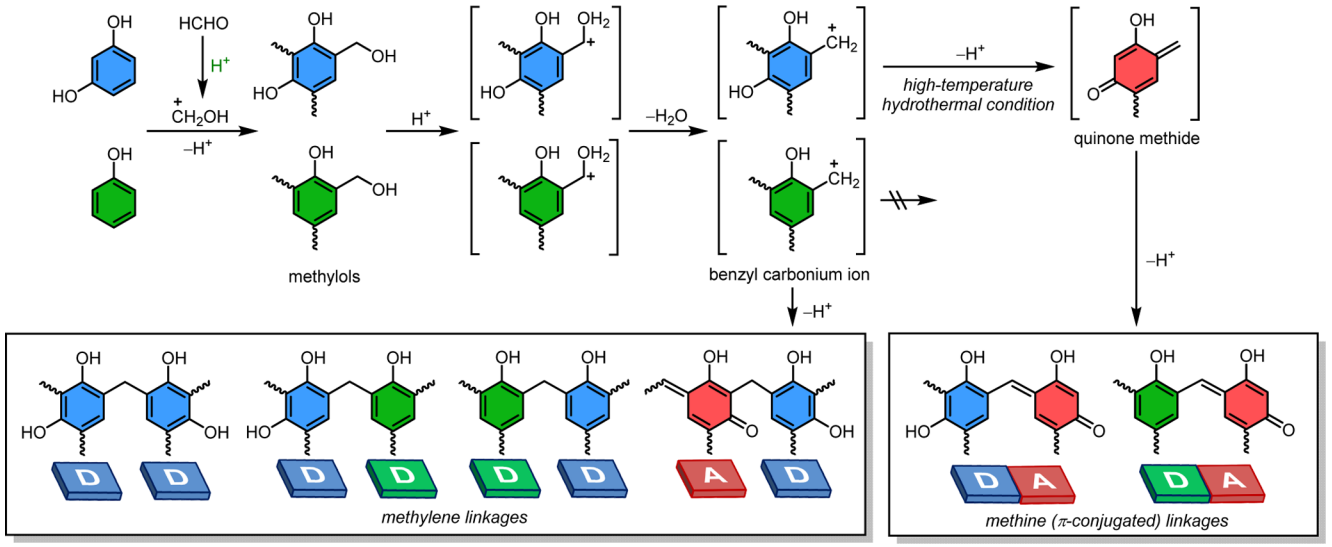

the resins prepared with larger amounts of phenol ($x \geq 20$) contained fewer A units (Table 1). This lowers the e^- conductivity of the resins (Figure 1e) and decreases the photocatalytic activity (Figure 1d).

Strengthened D–A π-Stacking

The e^- conductivity enhanced by incorporating a small amount of phenol (D) units ($x \leq 10$) within the resin originates from the strengthened D–A π-stacking. This was confirmed by powder XRD (Figure 1f). RF shows a broad peak at $2\theta = \sim 21.3°$ ($d_{002} = \sim 4.3$ Å) assigned to the π-stacked D–A units.[15] Adding small amounts of phenol leads to a shift of this peak to higher angles, which is indicative of a shortened π-stacking distance. The d_{002} peak of $P_5R_{95}F$ appears at $2\theta = \sim 24.2°$ (~3.8 Å); the π-stacking distance is ~0.5 Å shorter than that of RF. However, the peak of the resins prepared with larger amounts of phenol ($x \geq 20$) shifted to lower angles because the D–A π-stacking was weakened as a result of fewer quinoid (A) units. The higher angle shift of the d_{002} peak by incorporating phenol is consistent with the increased e^- conductivity (Figure 1e) and photocatalytic activity (Figure 1d). Therefore, the D–A π-stacking strengthened by incorporating small amounts of phenol ($x \leq 10$) is crucial for enhancing the conductivity and photocatalytic activity.

In RF resins, the H-bonding interactions of a large number of resorcinol –OH groups restrict the arrangement of the aromatic units, resulting in weaker D–A π-stacking. Incorporating small amounts of phenol (D) bearing a single –OH group in the resin relaxes this restriction and strengthens the D–A π-stacking. This was indicated by DFT calculations of vertically arranged simple A–D–A/D–A–D π-stacking

https://doi.org/10.1021/acsmaterialsau.2c00041
ACS Mater. Au 2022, 2, 709–718

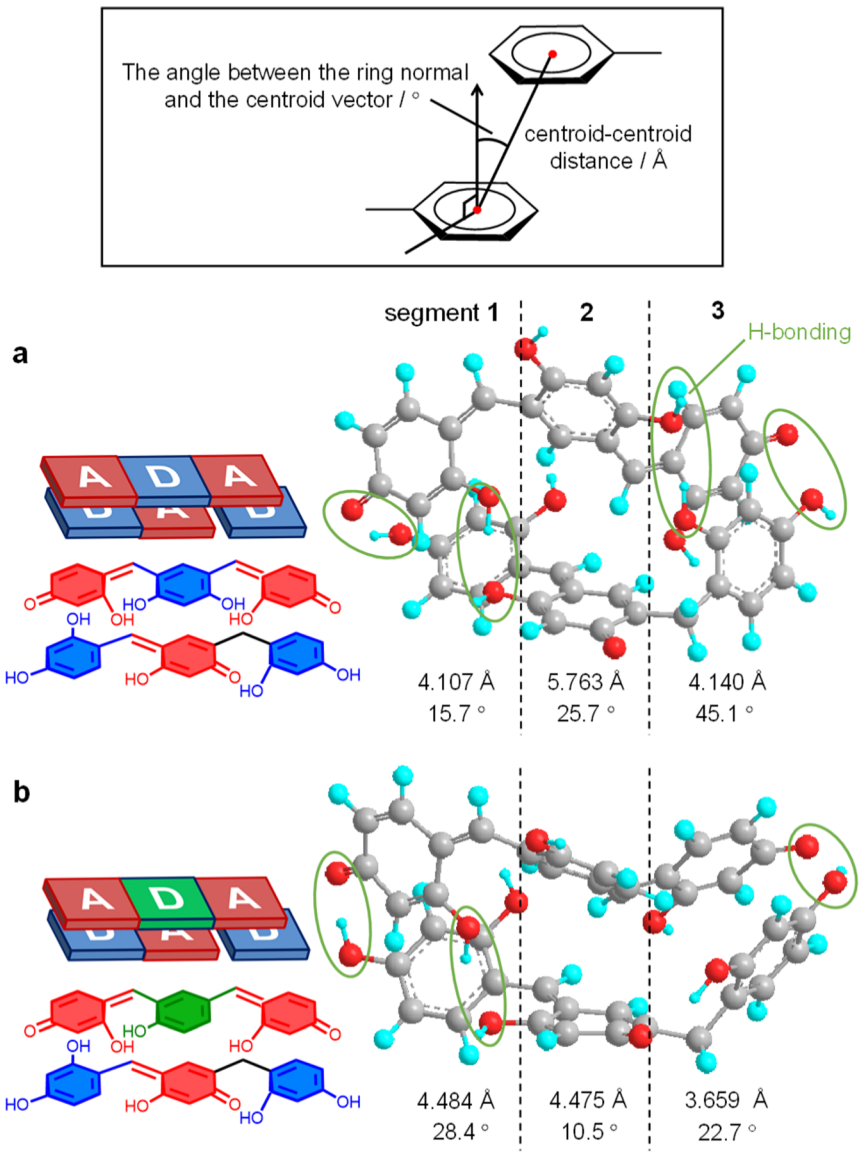

Figure 3. Optimized structures of the (a) all resorcinol A−D−A/D−A−D π-stacking model and (b) phenol-replaced A−D−A/D−A−D π-stacking model (DFT/B3LYP-D2/6-31+G*). The centroid−centroid distances and the angles between the ring normal and the centroid vectors for the respective D−A segments are denoted here.

models using a dispersion correction parameter (Figures S11 and S12).[34] Figure 3a shows the optimized structure of the model, which consists of resorcinol units, where the three sets of the D−A units arranged vertically (segments 1−3) are associated via π-stacking. Many of the −OH groups are associated with the H-bonding interactions, and aromatic rings are separated from each other, thereby creating slip-stacked configurations. The distance and angle between the aromatic rings affect the strength of π-stacking (Figure 3, top).[35] The average centroid−centroid distances and the angles for the three sets of the D−A units are 4.67 Å and 28.8°, respectively. In contrast, replacing the resorcinol D unit in the top A-D-A moiety with a phenol D unit (Figure 3b) brings the aromatic rings closer because one less −OH group weakens the H-bonding interactions and relaxes the restriction on the arrangement of the aromatic rings. The average distance and angle of the model decreased to 4.21 Å and 20.5°, respectively, confirming the strengthened π-stacking. Note that the difference in the average centroid−centroid distance in the two models (~0.46 Å) is similar to the d_{200} difference between the RF and $P_5R_{95}F$ resins (~0.5 Å), as determined by XRD (Figure 1f). This suggests that incorporating phenol bearing a single −OH group reduces the H-bonding interactions and strengthens the π-stacking between the D−A units. This, in turn, connects the dissipated semiconducting bands (Scheme 1e) and enhances the e^- conductivity of the resins.

The phenol (D) units are homogeneously incorporated within the resin particles. The surface C and O compositions of $P_5R_{95}F$ and $P_{50}R_{50}F$ determined by XPS are almost similar to the bulk C and O compositions determined by the combustion method (Table S2), as is the case for RF and PF.[36] The actual amounts of phenol incorporated in the $P_5R_{95}F$ and $P_{50}R_{50}F$ resins can be determined by a liquid chromatography analysis of the phenol/resorcinol mixtures before and after the hydrothermal treatment (Figure S13). The mole ratios of phenol/resorcinol incorporated within the resins are 3.4/96.6 for $P_5R_{95}F$ and 38.3/61.7 for $P_{50}R_{50}F$ (Table S3), respectively, which indicate that phenol is incorporated in less than its

https://doi.org/10.1021/acsmaterialsau.2c00041
ACS Mater. Au 2022, 2, 709−718

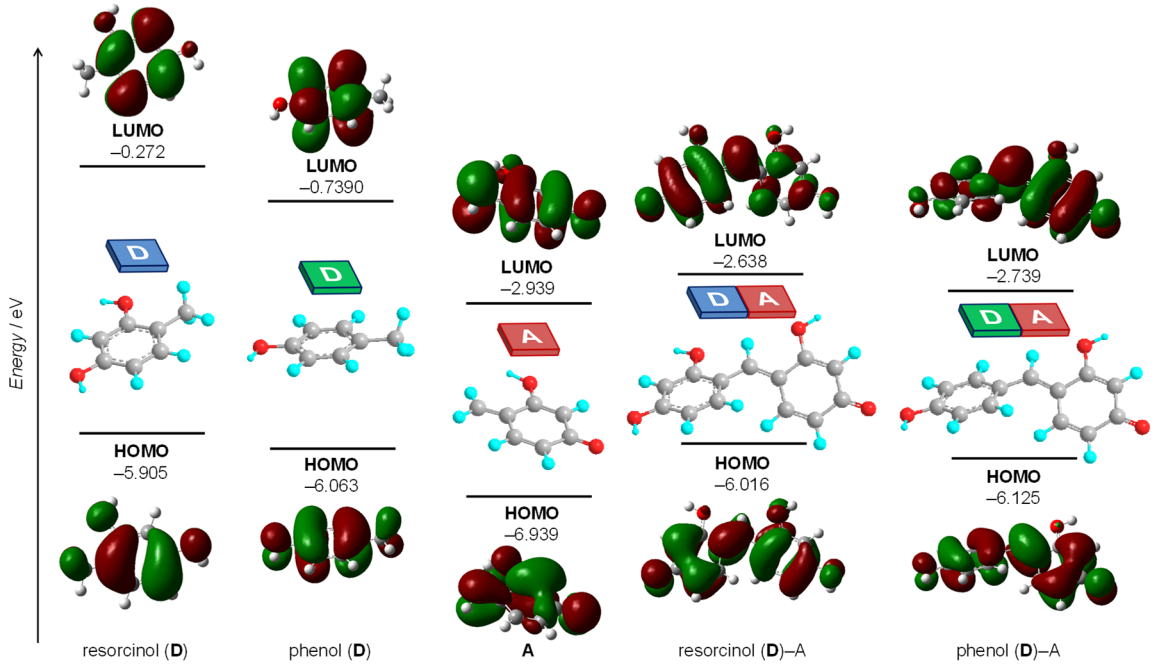

Figure 4. Energy diagrams and main molecular orbitals of the models (TD-DFT/B3LYP-D2/6-31+G*).

stoichiometric amounts within the resins due to its lower activity for polycondensation. Therefore, the active $P_5R_{95}F$ resin contains ~3 mol % phenol (D), which is homogeneously distributed within the resin particles and strengthened the π-stacking interaction.

Electronic Properties of the Resins

The Mott–Schottky (Figure S14) and Tauc plots (Figure S15) were used to determine the electronic band structures of the resins (Figure 1g). The E_{bg} values of RF (1.50 eV) and $P_5R_{95}F$ (1.54 eV) are similar, but the VB level (+1.93 V vs RHE) of $P_5R_{95}F$ lies at a potential ~0.2 eV lower than that of RF. $P_{50}R_{50}F$ had a larger E_{bg} (1.82 eV) and a further positively shifted VB level (+2.24 V). This positive VB shift by incorporating phenol originates from the HOMO level of the phenol (D) unit, which lies at a level lower than that of the resorcinol (D) unit. This was confirmed by time-dependent DFT (TD-DFT) calculations of the simple π-conjugated resorcinol (D)–A and phenol (D)–A couples (Figures S16–S20), where the singlet electronic excitations of all models mainly consisted of the HOMO → LUMO transition (Table S4). The HOMO of phenol (D) was lower than that of resorcinol (D) owing to its lower electron density (Figure 4). As a result of this, the HOMO of the hybridized phenol (D)–A couple lies at a level lower than that of the resorcinol (D)–A couple. The TD-DFT data agree well with the band structures of the resins (Figure 1g), clearly indicating that the incorporated phenol (D) units also contribute to the VB of the resins (Scheme 1f).

The action spectra for H_2O_2 generation obtained under monochromated light (Figure S21) indicate that the apparent quantum yields (Φ_{AQY}) on the $P_5R_{95}F$ resin are higher than those on RF over the entire wavelength range. This confirms that the e^- conductivity, enhanced by incorporating small amounts of phenol, promotes efficient h^+–e^- separation upon photoexcitation over the entire wavelength range. This enhances water oxidation (eq 1) and O_2 reduction (eq 2) on the $P_5R_{95}F$ resin. Half photoreactions using the sacrificial reagents confirmed this: the photoirradiation of $P_5R_{95}F$ in water containing benzyl alcohol as an e^- donor with O_2 generated H_2O_2 with higher activity than RF (Figure S22); also, the photoirradiation of $P_5R_{95}F$ in water with $NaIO_3$ as an e^- acceptor produced O_2 with higher activity than RF (Figure S23). Linear sweep voltammetry (LSV) measurements of the resins (Figure S24) exhibited a cathodic current at <0.5 V (vs RHE) for the O_2 reduction and an anodic current at >1.7 V (vs RHE) for the water oxidation, where both currents on $P_5R_{95}F$ are larger than those on RF. The results clearly indicate that water oxidation and O_2 reduction efficiently proceed owing to the enhanced h^+–e^- separation on the PRF resin.

H_2O_2 is generated through direct or indirect two-electron reduction of O_2 by the CB e^-,[8,9] where the indirect pathway involves the formation of a superoxide radical ($^\bullet$OOH) via one-electron reduction of O_2. Electron spin resonance (ESR) analysis using 5,5-dimethyl-1-pyrroline *N*-oxide (DMPO) as a spin trapping reagent was performed (Figure S25). An aqueous solution containing DMPO was photoirradiated with the catalyst under O_2. The resulting solution obtained with RF or $P_5R_{95}F$ shows almost no signal, although the solution obtained with TiO_2 shows signals assigned to the DMPO–$^\bullet$OOH adduct.[37] This implies that, on the RF resins, H_2O_2 may form via the direct two-electron reduction mechanism. Figure S26 shows the effect of reaction temperature on the photocatalytic H_2O_2 generation on the $P_5R_{95}F$ resin. The amounts of H_2O_2 generated at 298, 313, and 333 K are similar, indicating that the photocatalytic activity of the resin is scarcely affected at this temperature range. Figure S27 shows the effect of photoirradiation of $P_5R_{95}F$ in a H_2O_2 solution containing $NaIO_3$ as an electron acceptor under Ar. The activity for the oxidative decomposition of H_2O_2 by VB h^+ (the reverse reaction in eq 2) is similar to that on RF.[16] This indicates that the $P_5R_{95}F$ is also less active for subsequent H_2O_2 decomposition and this property also contributes to efficient H_2O_2 production.

https://doi.org/10.1021/acsmaterialsau.2c00041
ACS Mater. Au 2022, 2, 709–718

Artificial Photosynthesis Activities of the Resins

The artificial photosynthesis performance of the $P_5R_{95}F$ resin was also evaluated. Figure 5a shows the change in the amount

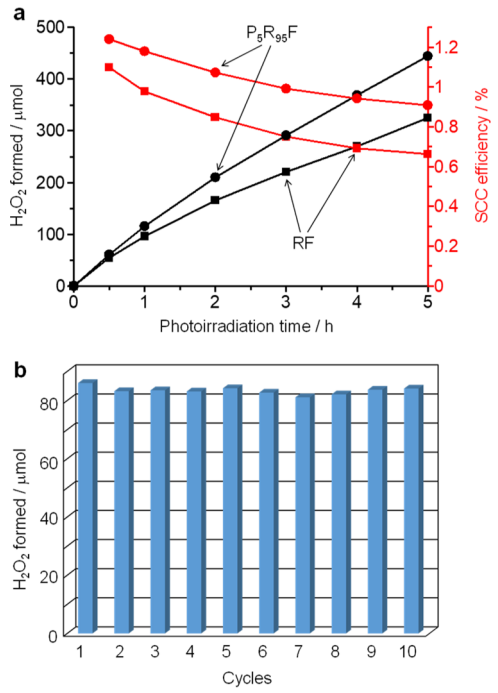

Figure 5. (a) Amount of H_2O_2 formed on the respective resins and SCC efficiency under the irradiation of AM 1.5G simulated sunlight (1 sun). Reaction conditions: water (50 mL), catalyst (150 mg), O_2 (1 bar), and temperature (333 K). Δ_rG at 333 K (=115.3 kJ mol^{-1}) was used for the SCC calculation (see Experimental Procedure in the Supporting Information). (b) Amount of H_2O_2 produced during repeated photoreaction using the $P_5R_{95}F$ resin. The resin after 5 h of photoirradiation (a) was collected by centrifugation and subjected to sequential photoreaction (1 h).

of H_2O_2 produced under AM 1.5G (1 sun) simulated sunlight irradiation[38] (Figure S5). The rate of H_2O_2 generation on $P_5R_{95}F$ was higher than that on RF, further verifying the positive effects of phenol incorporation. As in the case of RF, the high initial H_2O_2 generation rate for $P_5R_{95}F$ became constant after prolonged photoirradiation (~3 h). Therefore, the SCC efficiency of the H_2O_2 generation also becomes constant at ~0.9%, which is higher than that obtained with RF (~0.7%)[16] and is similar to that obtained with the RF/P3HT resin (~1.0%).[17] This confirms that the simple phenol incorporation into the RF resin is also effective for enhanced artificial photosynthesis of H_2O_2. It must also be noted that the SCC efficiency (~0.9%) is much higher than that obtained in the previously reported photocatalytic systems (<0.61%; Table S5). In contrast, in regard to the rate of H_2O_2 generation (μmol g^{-1} h^{-1}), some other systems show a higher generation rate than that of the present system (Table S5), although the rate depends on several factors (light source, irradiation area, catalyst amount, and reaction time for the rate determination), and it is difficult to compare the rates obtained under different conditions.

The high activity seen immediately after photoirradiation (Figure 5a) is because the photoformed VB h^+ is consumed not only by the water oxidation (eq 1) but also by self-oxidation of the resin, as observed for RF.[15,16] Table 1 shows the carbon composition of the $P_5R_{95}F$ resin after 5 h of photoreaction, as determined by NMR (Figure S8). Photoirradiation decreases the number of methylene and methylol carbons and increases the number of aldehyde and ketone carbons, indicating that VB h^+ oxidizes the methylol and methylene units (**j**, **k**, **l**, **i**) to the corresponding aldehyde and ketone units (**a**, **n**) (Figure 2).[15] However, the benzenoid/quinoid ratio (52/48) (Table 1), DR UV−vis spectrum (Figure 1a), and XRD pattern (Figure 1f) of the resin were almost unchanged even after the photoreaction. In addition, the recovered resin consists of spherical particles with a size (3.1 μm) similar to that of the fresh resin (2.9 μm) (Figures S1 and S3). Furthermore, even after 10 reuse cycles, the resin maintained high photocatalytic activity (Figure 5b). These data demonstrate that the morphology and performance of the $P_5R_{95}F$ resin did not change during the photoreaction, thereby promoting stable H_2O_2 generation.

CONCLUSIONS

We demonstrated that PRF resins containing small amounts of phenol prepared under high-temperature hydrothermal conditions behave as highly active photocatalysts for H_2O_2 generation from water and O_2. Incorporating phenol bearing a single −OH group into the RF resin matrices relaxes the restriction on the arrangement of the aromatic rings originating from the H-bonding interactions of the large number of resorcinol −OH groups. This creates stronger D−A π-stacking and enhances the e^- conductivity of the resins. The PRF resin stably generated H_2O_2 with more than 0.9% SCC efficiency, which is comparable to the highest efficiency among the previously reported systems. The simple catalyst design presented here, based on the incorporation of cost-effective phenol into the RF resin matrices, may contribute to the fabrication of highly conductive semiconductors and to the development of powder photocatalysts for solar-driven production of liquid fuels.

ASSOCIATED CONTENT

Supporting Information

The Supporting Information is available free of charge at https://pubs.acs.org/doi/10.1021/acsmaterialsau.2c00041.

Experimental procedure; SEM; TEM; DLS; N_2 adsorption/desorption; light emission spectra; photocurrent; IR; NMR; XPS; Cartesian coordinates of π-stacked models; LC chromatograms; Mott−Schottky plots; Tauc plots; Cartesian coordinates of D, A, and D−A couples; action spectra; half reaction for H_2O_2 formation; half reaction for O_2 formation; LSV charts; ESR; effect of reaction temperature; H_2O_2 decomposition; C═O and C−O compositions; C and O compositions; phenol/resorcinol ratio; TD-DFT results; and comparison of the photocatalytic performance (PDF)

AUTHOR INFORMATION

Corresponding Author

Yasuhiro Shiraishi − *Research Center for Solar Energy Chemistry, and Division of Chemical Engineering, Graduate School of Engineering Science, Osaka University, Toyonaka 560-8531, Japan; Innovative Catalysis Science Division, Institute for Open and Transdisciplinary Research Initiatives*

https://doi.org/10.1021/acsmaterialsau.2c00041
ACS Mater. Au 2022, 2, 709−718

(ICS-OTRI), Osaka University, Suita 565-0871, Japan; orcid.org/0000-0003-1812-0644;
Email: shiraishi.yasuhiro.es@osaka-u.ac.jp

Authors

Kanako Miura − *Research Center for Solar Energy Chemistry, and Division of Chemical Engineering, Graduate School of Engineering Science, Osaka University, Toyonaka 560-8531, Japan*

Masahiro Jio − *Research Center for Solar Energy Chemistry, and Division of Chemical Engineering, Graduate School of Engineering Science, Osaka University, Toyonaka 560-8531, Japan*

Shunsuke Tanaka − *Department of Chemical, Energy, and Environmental Engineering, Kansai University, Suita 564-8680, Japan;* orcid.org/0000-0001-5157-3317

Satoshi Ichikawa − *Research Center for Ultra-High Voltage Electron Microscopy, Osaka University, Ibaraki 567-0047, Japan*

Takayuki Hirai − *Research Center for Solar Energy Chemistry, and Division of Chemical Engineering, Graduate School of Engineering Science, Osaka University, Toyonaka 560-8531, Japan*

Complete contact information is available at: https://pubs.acs.org/10.1021/acsmaterialsau.2c00041

Author Contributions

All authors contributed equally. CRediT: **Yasuhiro Shiraishi** conceptualization (equal), funding acquisition (equal), investigation (equal), methodology (equal), project administration (equal), resources (equal), software (equal), supervision (equal), validation (equal), visualization (equal), writing-review & editing (equal); **Kanako Miura** data curation (equal), formal analysis (equal), investigation (equal), methodology (equal), writing-original draft (equal); **Masahiro Jio** data curation (equal), formal analysis (equal), investigation (equal), visualization (equal); **Shunsuke Tanaka** data curation (equal), formal analysis (equal), investigation (equal); **Satoshi Ichikawa** data curation (equal), formal analysis (equal), investigation (equal); **Takayuki Hirai** investigation (equal), supervision (equal), writing-review & editing (equal).

Notes

The authors declare no competing financial interest.

■ ACKNOWLEDGMENTS

This work was supported by a Grant-in-Aid for Scientific Research (nos. 20H05100 and 22H01867) and Nanotechnology Platform Project (nos. JPMXP09A20OS0032 and JPMXP09A21OS0005) from the Ministry of Education, Culture, Sports, Science and Technology, Japan (MEXT).

■ REFERENCES

(1) Chen, S.; Takata, T.; Domen, K. Particulate photocatalysts for overall water splitting. *Nat. Rev. Mater.* **2017**, *2*, 17050.
(2) Hisatomi, T.; Domen, K. Reaction systems for solar hydrogen production via water splitting with particulate semiconductor photocatalysts. *Nat. Catal.* **2019**, *2*, 387−399.
(3) Kondratenko, E. V.; Mul, G.; Baltrusaitis, J.; Larrazábal, G. O.; Pérez-Ramírez, J. Status and perspectives of CO_2 conversion into fuels and chemicals by catalytic, photocatalytic and electrocatalytic processes. *Energy Environ. Sci.* **2013**, *6*, 3112−3135.
(4) White, J. L.; Baruch, M. F.; Pander, J. E., III; Hu, Y.; Fortmeyer, I. C.; Park, J. E.; Zhang, T.; Liao, K.; Gu, J.; Yan, Y.; Shaw, T. W.; Abelev, E.; Bocarsly, A. B. Light-driven heterogeneous reduction of carbon dioxide: photocatalysts and photoelectrodes. *Chem. Rev.* **2015**, *115*, 12888−12935.
(5) Chen, X.; Li, N.; Kong, Z.; Ong, W. J.; Zhao, X. Photocatalytic Fixation of Nitrogen to Ammonia: State-of-the-Art Advancements and Future Prospects. *Mater. Horiz.* **2018**, *5*, 9−27.
(6) Li, M.; Huang, H.; Low, J.; Gao, C.; Long, R.; Xiong, Y. Recent Progress on Electrocatalyst and Photocatalyst Design for Nitrogen Reduction. *Small Methods* **2018**, *3*, 1800388.
(7) Fukuzumi, S. Production of Liquid Solar Fuels and Their Use in Fuel Cells. *Joule* **2017**, *1*, 689−738.
(8) Hou, H.; Zeng, X.; Zhang, X. Production of Hydrogen Peroxide by Photocatalytic Processes. *Angew. Chem., Int. Ed.* **2020**, *59*, 17356−17376.
(9) Hu, X.; Zeng, X.; Liu, Y.; Lu, J.; Zhang, X. Carbon-Based Materials for Photo- and Electrocatalytic Synthesis of Hydrogen Peroxide. *Nanoscale* **2020**, *12*, 16008−16027.
(10) Sun, Y.; Han, L.; Strasser, P. A Comparative Perspective of Electrochemical and Photochemical Approaches for Catalytic H_2O_2 Production. *Chem. Soc. Rev.* **2020**, *49*, 6605−6631.
(11) Pekala, R. W. Organic aerogels from the polycondensation of resorcinol with formaldehyde. *J. Mater. Sci.* **1989**, *24*, 3221−3227.
(12) Al-Muhtaseb, S. A.; Ritter, J. A. Preparation and properties of resorcinol-formaldehyde organic and carbon gels. *Adv. Mater.* **2003**, *15*, 101−114.
(13) ElKhatat, A. M.; Al-Muhtaseb, S. A. Advances in Tailoring Resorcinol-Formaldehyde Organic and Carbon Gels. *Adv. Mater.* **2011**, *23*, 2887−2903.
(14) Durairaj, R. B. *Resorcinol, Chemistry, Technology and Applications*; Springer-Verlag Berlin Heidelberg: New York, 2005.
(15) Shiraishi, Y.; Takii, T.; Hagi, T.; Mori, S.; Kofuji, Y.; Kitagawa, Y.; Tanaka, S.; Ichikawa, S.; Hirai, T. Resorcinol-Formaldehyde Resins as Metal-Free Semiconductor Photocatalysts for Solar-to-Hydrogen Peroxide Energy Conversion. *Nat. Mater.* **2019**, *18*, 985−993.
(16) Shiraishi, Y.; Hagi, T.; Matsumoto, M.; Tanaka, S.; Ichikawa, S.; Hirai, T. Solar-to-hydrogen peroxide energy conversion on resorcinol-formaldehyde resin photocatalysts prepared by acid-catalysed polycondensation. *Commun. Chem.* **2020**, *3*, 169.
(17) Shiraishi, Y.; Matsumoto, M.; Ichikawa, S.; Tanaka, S.; Hirai, T. Polythiophene-Doped Resorcinol-Formaldehyde Resin Photocatalysts for Solar-to-Hydrogen Peroxide Energy Conversion. *J. Am. Chem. Soc.* **2021**, *143*, 12590−12599.
(18) Burattini, S.; Greenland, B. W.; Merino, D. H.; Weng, W.; Seppala, J.; Colquhoun, H. M.; Hayes, W.; Mackay, M. E.; Hamley, I. W.; Rowan, S. J. A Healable Supramolecular Polymer Blend Based on Aromatic $\pi-\pi$ Stacking and Hydrogen-Bonding Interactions. *J. Am. Chem. Soc.* **2010**, *132*, 12051−12058.
(19) Hirschberg, J. H. K. K.; Brunsveld, L.; Ramzi, A.; Vekemans, J. A. J. M.; Sijbesma, R. P.; Meijer, E. W. Helical Self-Assembled Polymers from Cooperative Stacking of Hydrogen-Bonded Pairs. *Nature* **2000**, *407*, 167−170.
(20) Dinwoodie, J. M. In *Wood Adhesives Chemistry and Technology*; Pizzi, A., Ed.; Marcel Dekker: New York, 1983; Vol. *1*, Chapter 1.
(21) Tohmura, S. I.; Miyamoto, K.; Inoue, A. Acetaldehyde Emission from Glued-Laminated Timber Using Phenol-Resorcinol-Formaldehyde Resin Adhesives with Addition of Ethanol. *J. Wood Sci.* **2005**, *51*, 421−423.
(22) Christiansen, A. W. How Overdrying Wood Reduces Its Bonding To Phenol-Formaldehyde Adhesives: A Critical Review of the Literature. Part I. Physical Responses. *Wood Fiber Sci.* **1990**, *22*, 441−459.
(23) Scopelitis, E.; Pizzi, A. The Chemistry and Development of Branched PRF Wood Adhesives of Low Resorcinol Content. *J. Appl. Polym. Sci.* **1993**, *47*, 351−360.
(24) Badhe, Y.; Balasubramanian, K.; Gupta, R. Cost-Effective, Low Density, Carbon Soot Doped Resorcinol Formaldehyde Composite for Ablative Applications. *RSC Adv.* **2015**, *5*, 23622−23634.

(25) Nada, A. M. A.; Fadly, M.; Dawy, M. Spectroscopic Study of the Molecular Structure of a Lignin-Polymer System. *Polym. Degrad. Stab.* **1992**, *37*, 125−129.
(26) Kim, M. G.; Amos, L. W.; Barnes, E. E. Investigation of a resorcinol-formaldehyde resin by 13C-NMR spectroscopy and intrinsic viscosity measurement. *J. Polym. Sci., Part A: Polym. Chem.* **1993**, *31*, 1871−1877.
(27) Šebenik, A.; Osredkar, U.; Vizovišek, I. Study of the reaction between resorcinol and formaldehyde. *Polymer* **1981**, *22*, 804−806.
(28) Gutiérrez, M. C.; Rubio, F.; del Monte, F. Resorcinol-Formaldehyde Polycondensation in Deep Eutectic Solvents for the Preparation of Carbons and Carbon−Carbon Nanotube Composites. *Chem. Mater.* **2010**, *22*, 2711−2719.
(29) Liebscher, J.; Mrówczyński, R.; Scheidt, H. A.; Filip, C.; Turcu, R.; Bende, A.; Beck, S. Structure of Polydopamine: A Never-Ending Story? *Langmuir* **2013**, *29*, 10539−10548.
(30) del Valle, M. A.; Herrera, F. V.; Díaz, F. R.; Capurro, C.; Durán, M.; East, G. A. Electropolymerization of *N*-vinylcarbazole in the presence of Galvinoxyl. *Polym. Bull.* **2006**, *57*, 321−328.
(31) Zafra, M. C.; Lavela, P.; Rasines, G.; Macías, C.; Tirado, J. L. Effect of the Resorcinol/Catalyst Ratio in the Capacitive Performance of Carbon Xerogels with Potential Use in Sodium Chloride Removal from Saline Water. *J. Solid State Electrochem.* **2014**, *18*, 2847−2856.
(32) Mulik, S.; Sotiriou-Leventis, C.; Leventis, N. Time-Efficient Acid-Catalyzed Synthesis of Resorcinol−Formaldehyde Aerogels. *Chem. Mater.* **2007**, *19*, 6138−6144.
(33) Li, T.; Cao, M.; Liang, J.; Xie, X.; Du, G. Theoretical Confirmation of the Quinone Methide Hypothesis for the Condensation Reactions in Phenol-Formaldehyde Resin Synthesis. *Polymers* **2017**, *9*, 45.
(34) Grimme, S. Semiempirical GGA-Type Density Functional Constructed with a Long-Range Dispersion Correction. *J. Comput. Chem.* **2006**, *27*, 1787−1799.
(35) Janiak, C. A critical account on π-π stacking in metal complexes with aromatic nitrogen-containing ligands. *J. Chem. Soc., Dalton Trans.* **2000**, 3885−3896.
(36) Wagner, C. D.; Davis, L. E.; Zeller, M. V.; Taylor, J. A.; Raymond, R. H.; Gale, L. H. Empirical Atomic Sensitivity Factors for Quantitative Analysis by Electron Spectroscopy for Chemical Analysis. *Surf. Interface Anal.* **1981**, *3*, 211−225.
(37) Shiraishi, Y.; Kanazawa, S.; Sugano, Y.; Tsukamoto, D.; Sakamoto, H.; Ichikawa, S.; Hirai, T. Highly Selective Production of Hydrogen Peroxide on Graphitic Carbon Nitride ($g\text{-}C_3N_4$) Photocatalyst Activated by Visible Light. *ACS Catal.* **2014**, *4*, 774−780.
(38) Gordon, I.; Krebs, F. C.; Mathew, X.; Lampert, C. M.; Rougier, A.; Smestad, G. P.; Subrahmanyam, A. Editorial. *Sol. Energy Mater. Sol. Cells* **2015**, *133*, A1−A6.

https://doi.org/10.1021/acsmaterialsau.2c00041
ACS Mater. Au 2022, 2, 709−718